International Research Journal of Engineering and Technology (IRJET) e-ISSN: 2395-0056
Volume: 04 Issue: 07 | July -2017 www.irjet.net p-ISSN: 2395-0072

Synthesis, Spectroscopic (FT-IR, FT-Raman), first order hyperpolarizability and HOMO-LUMO analysis of (2E)-N-phenyl-3-(4H-pyran-4-yl) prop-2-enamide

S. Abbas Manthiri[1], R. Raj Muhamed[1*], V. Sathyanarayanamoorthi[2], R. Rajesh[3], M. Raja[1]

[1]Department of Physics, Jamal Mohamed College, Tiruchirappalli-620020, Tamil Nadu, India
[2]Post Graduate and Research Department of Physics, PSG College of Arts and Science, Coimbatore-641014, India
[3]Post Graduate and Research Department of Physics, Sri Vijay Vidyalaya College of Arts and Science for Woman, Dharmapuri-636807, India

---

Abstract - *In this work, the vibrational spectral analysis was carried out by using FT-Raman and FT-IR spectroscopy in the range 4000-100 cm-1 and 4000-400 cm-1 respectively, for (2E)-N-phenyl-3-(4H-pyran-4-yl)prop-2-enamid (P3P2E) molecule. Theoretical calculations were performed by density functional theory (DFT) method using 6-311++G(d,p) basis sets. The complete vibrational assignments of wavenumbers were made on the basis of potential energy distribution (PED). The results of the calculations were applied to simulated spectra of the title compound, which show excellent agreement with observed spectra. The frontier orbital energy gap and dipole moment illustrates the high reactivity of the title molecule. The first order hyperpolarizability (β0) and related properties (μ, α and Δα) of the molecule were also calculated. Molecular electrostatic potential (MEP) and HOMO-LUMO energy levels are also constructed. The thermodynamic properties of the title compound were calculated at different temperatures.*

Key Words: DFT, FT-IR, FT-Raman, NLO, MEP

1. INTRODUCTION

Enamides or enecarbamates are well-known versatile motifs in organic synthesis [1,2]. The π-donating ability of their nitrogen atom renders enamines more electron-rich [3] than simple enols or enol ethers, thereby predisposing them to electrophilic activation. However, enamines are highly sensitive toward hydrolysis, thereby creating serious difficulties in their experimental handling [4,5]. Consequently, the great potential of the chemistry of enamines has not been completely exploited. In this context, efforts have been directed towards the use of more stable enamines [6]. Enamides and enecarbamates that carry an electron-withdrawing group on the nitrogen were found to be ideal candidates. Indeed, enamides are commonly present in natural products and active drugs [7, 8] demonstrating their high stability.

The density functional theory (DFT) is a popular method for the calculation of molecular structures, vibrational frequencies and energies of molecules [6]. The density functional theory studies on the vibrational and electronic spectra of Enamides derivative (2E)-N-phenyl-3-(4H-pyran-4-yl)prop-2-enamid has not been carried out. Thus, in the present investigation, owing to the biological importance of substituted phenyl, an extensive experimental and theoretical studies of title compound has been undertaken by recording their FT-IR, FT-Raman spectra and subjecting them to potential energy distribution analysis for the proper assignment of the vibrational fundamentals. In addition, HOMO, LUMO analysis has been used to elucidate the information regarding charge transfer within the molecule.

2. METERIAL AND METHODS

2.1 Synthesis

A mixture of equimolar (0.01) concentration of finely powdered 1.35 g N-phenylacetamide and 1.10 g of 4H-pyran-4-carbaldehyde were dissolved in minimum amount of ethanol (30ml) taken in round bottom flask stir for 30 minutes. Sufficient 2N NaOH solution was added to the above solution and continuous stirring for 5 hrs in ice cold condition till yellow precipitate was formed. This was then neutralized with 2N HCl and dilutes with water and left overnight. The precipitate chalcones were filtered and washed with water and recrystallised from ethanol. The reaction scheme is given Fig 1

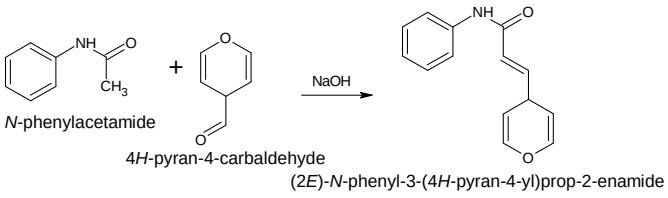

Fig -1: The scheme of the synthesis of P3P2E

2.2 Experimental details

The FT-IR spectrum of the synthesis compound (2E)-N-phenyl-3-(4H-pyran-4-yl)prop-2-enamid (P3P2E) was recorded in the region 4000-450 cm-1 in evacuation mode using a KBr pellet technique with 1.0 cm-1 resolution on a PERKIN ELMER FT-IR spectrophotometer. The FT-Raman

spectrum of the P3P2E compound was recorded in the region 4000-100 cm-1 in a pure mode using Nd: YAG Laser of 100 mW with 2 cm-1 resolution on a BRUCKER RFS 27 at SAIF, IIT, Chennai, India.

2.3 Computational details

For meeting the requirements of both accuracy and computing economy, theoretical methods and basis sets should be considered. DFT has proved to be extremely useful in treating electronic structure of the molecules. The molecular structure optimization of the title compound and corresponding vibrational harmonic frequencies were calculated using DFT with Becke-3-Lee-Yang–Parr (B3LYP) combined with standard 6-311++G(d,p) basis sets using Gaussian 09W program package without any constraint on the geometry [10]. The harmonic vibrational frequencies were calculated at the same level of theory for the optimized structures and obtained frequencies were scaled by 0.961 [11]. The spectra were analyzed in terms of the PED aid by using the VEDA program [12].

3. RESULTS AND DISCUSSION

3.1 Molecular geometry

The numbering system adopted in the molecular structure of P3P2E is shown in Fig. 2. The optimized structure parameters of this compound calculated DFT/B3LYP levels with the 6-311++G(d,p) basis set are listed in Table 1. Since the crystal structure of this P3P2E is not available in the literature. Therefore, the crystal data of a closely related molecule such as (E)-2-Cyano-3-[4-(dimethylamino)-phenyl]-N-phenylprop-2-enamide [13] is compared with that of the title compound. The theoretical calculations were carried out isolated molecule in the gaseous phase the experimental results are for a molecule in a solid state.

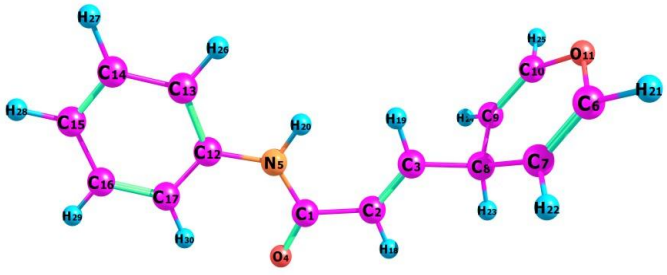

Fig -2: The theoretical optimized geometric structure with atoms numbering of P3P2E

This title molecule has thirteen C - C bond lengths, twelve C - H bond lengths, three (C-O), two C - N bond lengths and one N - H bond lengths respectively. The highest bond length was calculated for C3 – C8, C7 - C8 found to be 1.517 and 1.515 Å.The calculated bond length values for C-C and C-H in the benzene ring vary from 1.517-1.331 Å and 1.0869-1.081 Å by B3LYP/6-311G(d,p) basis set.

Table -1: Optimized geometrical parameters of P3P2E

Parameters	Exp[a]	B3LYP	Parameters	Exp[a]	B3LYP
Bond length(Å)			Bond angle(°)		
C1-C2	1.493	1.494	C2-C1-O4	120.5	119.6
C1-O4	1.216	1.223	C2-C1-N5	116.3	116.6
C1-N5	1.363	1.376	C1-C2-C3	131.6	128.9
C2-C3	1.349	1.335	C1-C2-H18	114	111.3
C2-H18	0.9600	1.086	O4-C1-N5	124	123.8
C3-C8	1.493	1.517	C1-N5-C12	128.4	129.3
C3-H19	0.9600	1.089	C1-N5-H20	116	116.2
N5-C12	1.422	1.411	C3-C2-H18	119	119.9
N5-H20	0.8600	1.008	C2-C3-C8	122.9	124.3
C6-C7	1.347	1.331	C2-C3-H19	120	121.9
C6-O11	1.216	1.373	C8-C3-H19	114	113.8
C6-H21	0.9600	1.081	C3-C8-C7	116.1	111.1
C7-C8	1.493	1.515	C3-C8-C9	116.1	111.1
C7-H22	0.9600	1.083	C3-C8-H23	114	107
C8-C9	1.493	1.515	C12-N5-H20	116	114.5
C8-H23	0.9600	1.098	N5-C12-C13	116.3	117.1
C9-C10	1.347	1.331	N5-C12-C17	124.7	123.6
C9-H24	0.9600	1.083	C7-C6-O11	121.2	124.8
C10-O11	1.216	1.373	C7-C6-H21	120	124.3
C10-H25	0.9600	1.081	C6-C7-C8	122.9	122.9
C12-C13	1.407	1.403	C6-C7-H22	119	118.4
C12-C17	1.407	1.401	O11-C6-H21	-	110.9
C13-C14	1.397	1.389	C6-O11-C10	121	116
C13-H26	0.9600	1.086	C8-C7-H22	119	118.8
C14-C15	1.397	1.395	C7-C8-C9	116.1	108.4
C14-H27	0.9600	1.084	C7-C8-H23	114	109.6
C15-C16	1.397	1.393	C9-C8-H23	114	109.6
C15-H28	0.9600	1.084	C8-C9-C10	122.9	122.9
C16-C17	1.397	1.394	C8-C9-H24	119	118.8
C16- H29	0.9600	1.084	C10-C9-H24	119	118.4
C17-H30	0.9600	1.079	C9-C10-O11	121.2	124.8
			C9-C10-H25	120	124.3
			O11-C10-H25	-	110.9
			C13-C12-C17	118.2	119.3
			C12-C13-C14	120.5	120.6
			C12-C13-H26	120	119.7
			C12-C17-C16	118.2	119.3
			C12-C17-H30	120	119.6
			C14-C13-H26	120	119.7
			C13-C14-C15	120.5	120.2
			C13-C14-H27	120	119.4
			C15-C14-H27	120	120.3
			C14-C15-C16	118.2	119.1
			C14-C15-H28	120	120.4
			C16-C15-H28	120	120.5
			C15-C16-C17	121.9	121.4
			C15-C16-H29	120	119.9
			C17-C16-H29	120	118.7
			C16-C17-H30	120	121.1

[a] Taken from Ref [13]

The C-C bond lengths are higher than the C-H bond lengths. The important reasons for the same charges are repulsive and opposite charges are attractive.

Based on the above comparison, although there are some differences between theoretically calculated values, these differences are probably due to intermolecular interaction in the solid state. All calculated geometrical

parameters obtained at the DFT level of theory are in good agreement with the experimental structural parameters

3.2 Vibrational analysis

The maximum number of potentially active observable fundamental of non-linear molecule, which contains N atoms, is equal to (3N-6) apart from three translational and three rotational degrees of freedom. The present molecule P3P2E with 30 atoms and 84 normal modes of vibrations has C1 point group symmetry. For visual comparison, the observed and calculated FT-IR and FT-Raman spectra of P3P2E are shown in Figs. 3 and 4 respectively. The detailed description of vibrational modes can be given by Potential energy distribution (PED). In The calculated vibrational frequencies (Unscaled and Scaled), IR intensity, Raman activity are tabulated in Table 2.

3.2.1 C-H vibrations

In the aromatic compounds, the C-H stretching wavenumbers appear in the range 3000-3100 cm^{-1} which are the characteristic region for the ready identification of C-H stretching vibrations [14]. The C-H stretching and bending regions are of the most difficult regions to interpret in infrared spectra. The nature and position of the substituent cannot affect these vibrations. Most of the aromatic compounds have almost four infrared peaks in the region 3080-3010 cm-1 due to ring C-H stretching bands [15]. In this present study, the C-H stretching vibrations are observed at 3119, 3096, 3067, 3044 and 2871 cm^{-1} by B3LYP/6-311++G(d,P) method show good agreements with experimental vibrations. The bands observed in the recorded FT-IR spectrum 3127(s), 3074(s), 2996(m), 2854(m) cm^{-1} and with the FT-Raman spectrum bands at 3128(s), 3095(s), 3043(vw), 2989(vw) cm^{-1}. The PED corresponding to this pure mode of title molecule contributed 99, 92, 99, 99, 99 and 100% is shown in Table 2.

3.2.2 C-C ring vibrations

The C-C stretching vibrations are expected in the range from 1650 to 1100 cm^{-1} which are not significantly influenced by the nature of the substituents [16]. The C-C stretching vibrations of the P3P2E compound were observed from1602 to 1082 cm^{-1}. In this present study, the C-C stretching vibrations are found at 1666(vs), 1608(vs), 1594(vs), 1393(vs), 1291(vs), 1259(vs), 1169(s), 1039(s), 1008(vs) 829(vs) cm-1 in FT-IR and 1688(s), 1663(vs), 1624(vw), 1592(vs), 1546(s), 1292(vs), 1010(vs) cm-1 in FT-Raman respectively. The theoretical wavenumbers at 1666, 1661, 1615, 1603, 1578, 1570, 1411, 1288, 1273, 1178, 1054, 1011 and 829 cm^{-1} are assigned as C-C stretching vibrations with PED contribution of 49, 40, 58, 40, 32, 44, 24, 22, 58, 19, 62, 45 and 22% respectively.

3.2.3 C-N vibrations

The C-N stretching frequency is a very tough task since it falls in a composite region of the vibrational spectrum, i.e., mixing of several bands are possible in this region [17] assigned C-N stretching absorption in the region 1386-1266 cm^{-1} for the aromatic compound. The bands observed at 1489(vs), 1169(s), 829(vs) cm^{-1} in FT-IR are assigned as C-N stretching vibrations. The theoretically scaled wavenumbers calculated at 1501, 1178, 829 cm^{-1} are assigned as C-N stretching vibrations with PED contribution of 24, 19 and 19% respectively.

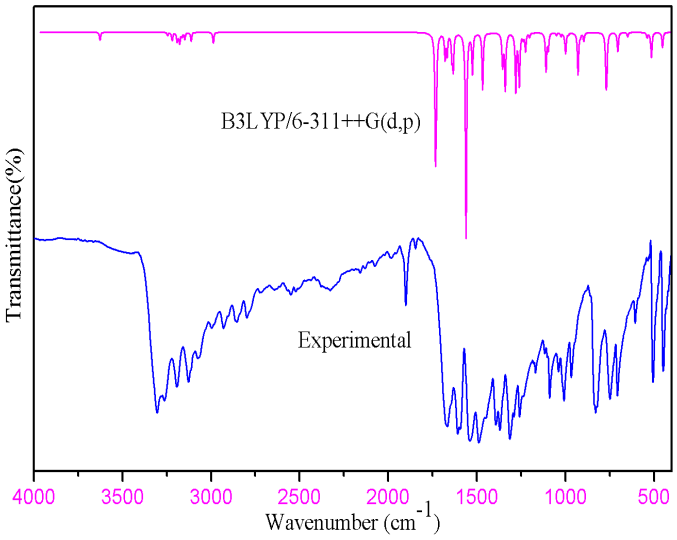

Fig -3: Experimental and theoretical FT-IR spectra of P3P2E

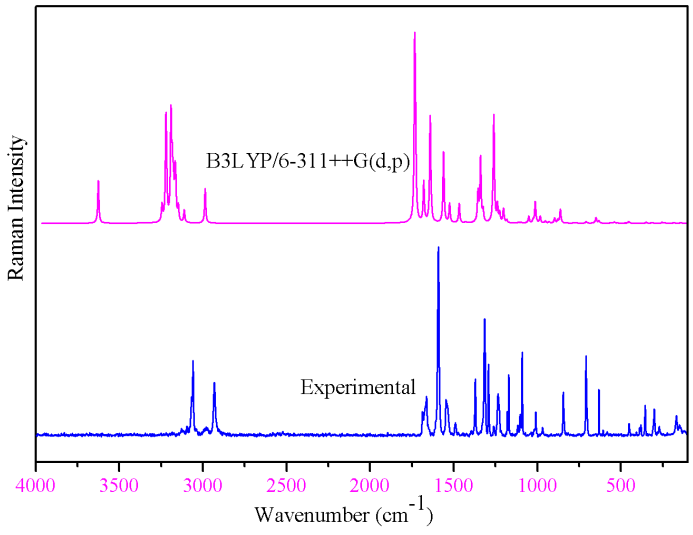

Fig -4: Experimental and theoretical FT-Raman spectra of P3P2E

Table -2: Calculated vibrational frequencies (cm-1) assignments of P3P2E based on B3LYP/6-311++G(d,p)
aγ-stretching,γa-Symmetrical stretching,γas-asymmetrical stretching, β- bending , τ-torsion, vs-very strong, s- strong, m-

Mode no	Experimental wave number (cm-1)		Theoretical wave number(cm-1)		I_{IR} [c]	I_{RAMAN} [d]	Assignments (PED)[a,b]
	FTIR	FT-RAMAN	Unscaled	scaled			
84	-	-	3626	3485	4	26	γNH(100)
83	3127(s)	3128(s)	3245	3119	2	10	γCH (99)
82	-	3095(s)	3222	3096	1	52	γCH (92)
81	-	-	3219	3093	4	20	γCH (92)
80	3074(s)	-	3192	3067	4	61	γCH (99)
79	-	-	3184	3060	0	16	γCH (92)
78	-	-	3184	3059	1	12	γCH (92)
77	-	-	3177	3053	5	19	γCH (99)
76	-	3043(vw)	3168	3044	0	20	γCH (99)
75	-	-	3164	3040	2	18	γCH (99)
74	-	-	3148	3025	3	9	γCH (90)
73	2996(m)	2989(vw)	3112	2991	4	7	γCH (99)
72	2854(m)	2981(s)	2987	2871	5	21	γCH (100)
71	1666(vs)	1688(s)	1734	1666	56	100	γOC (46) + γCC (49)
70	-	1663(vs)	1729	1661	24	39	γOC (46) + γCC (40)
69	1608(vs)	1624(vw)	1680	1615	12	24	γOC (46) + γCC (58)
68	1594(vs)	-	1668	1603	10	1	γCC (40)
67		1592(vs)	1642	1578	11	64	γCC (32)
66	-	1546(s)	1634	1570	17	3	γCC (44) + βHNC(43)
65	1489(vs)	-	1562	1501	100	43	γNC (24) + βHNC(43)
64		1490(m)	1525	1466	19	11	βHCC(62)
63	1393(vs)	-	1468	1411	28	12	γCC (24) + βHCC(34)
62	1370(vs)	1372(vs)	1429	1373	0	1	βHCO(59)+ βHCC(47)
61	1314(vs)	1315(vs)	1375	1321	0	0	βHCO(59)
60	-	-	1357	1304	6	8	βHCC(86) + τHCCC(19)
59	-	-	1354	1301	11	12	βHCC(86) + τHCCC(19)
58	1291(vs)	1292(vs)	1340	1288	27	39	γCC (22) + βHCC(19)
57		1262(s)	1329	1277	1	1	βHCC(43) + τHCCC(19)
56	1259(vs)	-	1325	1273	0	7	γCC (58) + βHCC(73)
55	-	1236(s)	1281	1231	28	0	γOC (44) + βHCC(47)
54	-	-	1266	1217	4	6	γNC (19)+βHCC(30)+τHCCC(19)
53	-	-	1261	1212	24	63	γCC (14) + γNC (19) + βHNC(43)
52	-	1180(s)	1239	1191	3	10	βHCO(59)+ βHCC(47)
51	1169(s)	-	1226	1178	9	6	γNC (19) + γCC (19) + βHCC(30) + τHCCC(19)
50	-	-	1203	1156	2	8	βHCC(73)
49	1117(m)	1117(vs)	1183	1137	0	2	βHCC(64)
48	1089(vs)	1091(vs)	1112	1068	3	0	γCC (69) + βHCC(77)
47	-	-	1110	1067	16	0	γOC (21) +γCC (16) + βHCC(43)
46	1039(s)	-	1097	1054	8	0	γCC (62)
45	1008(vs)	1010(s)	1052	1011	1	4	γCC 45) + βHCC(11)
44	-		1026	986	2	2	βCCC(20)+ βCCO(31)
43	-		1013	974	0	13	βCCC(75)
42	967(s)	969(vs)	1006	967	1	0	τHCCN(32)+ τHCCC(41)
41	-		1003	964	0	0	τHCCC(94)+ τCCCC(11)
40	-		1000	961	10	0	γOC (23) + γCC (16) + τHCCN(32)
39	-		983	945	1	4	γNC (24) + γCC (19)
38	-		978	940	0	0	τHCCC(91)
37	-		960	922	0	0	τHCOC(62)+ τHCCO(62)
36	-		952	914	0	1	τHCOC(62)+ τHCCO(62)
35	-		930	894	21	1	γOC (44) + βCOC(23)
34	-		916	881	2	0	τHCCC(97)
33	-		897	862	4	3	γOC (44) + βOCC(41) + βCOC(23)
32	-	845(vs)	878	844	0	2	τHCCN(32)+ τHCCC(41)+Out ONCC(-20)
31	829(vs)		863	829	0	8	γCC (22) + γNC (19) +βCCC(26)+ βCCN(22)
30	-		841	808	0	0	τHCCC(99)
29	749(vs)		785	754	0	0	τHCOC(62)+ τHCCO(62)
28	-		772	741	21	0	τHCCO(62)
27	707(vs)		767	737	15	0	τHCCC(99)+ τCCCC(11)+Out NCCC(25)
26	-	709(vs)	707	680	1	1	βCCC(26)
25	-		707	680	1	0	τHCCN(32)+ τCCCC(31)+ Out ONCC(-20)
24	-		705	677	8	0	τHCCC(66)+ τCCCC(70)
23	-	632(vs)	650	624	2	3	τCCOC(19)+ τOCCC(-19)+ τCOCC(15)
22	-		648	623	0	1	βCCC(-13)+ βCCO(31)+ βOCC(41)
21	606(m)		632	607	0	1	βCCC(66)
20	535(w)		561	539	0	0	βCCC(39)+ βCOC(23)
19	-		540	519	2	1	βOCC(37)+ βCCC(17)+ βCOC(23)
18	506(s)		521	501	1	0	τHNCC(50)+Out NCCC(25)
17	-		515	495	12	0	τHNCC(50)+Out NCCC(25)
16	449(s)	451(m)	475	457	0	0	βCCC(14)+ τCCCC(43)+ τCCOC(19)+ τOCCC (-18)+ τCOCC(15)
15	-		453	435	7	1	βCCC(13)+ τCCOC(19)
14	-	381(s)	418	401	0	0	τHCCC(71)+ τCCCC(70)
13	-	355(s)	348	334	0	0	βCCC(17)+βCNC(26)+ βNCC(34)
12	-	301(s)	317	305	0	0	βCCC(14)+τOCCC(-18)+ τCCCC(31)
11	-		310	298	4	0	βOCC(37)+τCOCC(15)
10	-	271(vs)	253	243	0	0	τCCCC(70)+ τCCNC(15)
9	-		237	228	0	0	γCC (19) +βCCC(39)+ βCCN(22)
8	-	169(s)	182	175	1	0	βCCC(13)+βCNC(26)+ βNCC (34)
7	-	150(vs)	142	137	1	0	τCCCC(68)
6	-		89	85	0	0	βCCC(13)+βCNC(26)+ βCCN (22) +τCCCC(43)+ τCOCC(15)
5	-		56	54	1	0	τCNCC(45)+ τCCCC(68)
4	-		50	48	0	0	τCCCN(-17)+ τCNCC(45)+τCCCC(37)
3	-		37	36	0	1	τCCNC(51)+τCCCC(31)+OutNCCC(25)
2	-		37	36	0	1	βCCC(52)+τCCCC(43)
1	-		16	15	1	0	τCCCN(-17)+τCCOC(37)

medium, w-weak, vw-very weak.
[b]scaling factor : 0.961 for B3LYP/6-311+G(d,p)
[c]Relative absorption intensities normalized with highest peak absorption equal to 100.

3.2.4 C–O vibration

The C-O stretching vibration occurs at 1627 (vs) cm−1 in FT-IR and 1626 cm−1 in solid FT-Raman [18]. Normally, the C–O stretching vibrations occur in the region 1260-1000 cm-1 [19]. The C-C stretching vibrations of the P3P2E compound were observed from1690 to 1230 cm^{-1}. In this present study, the C-C stretching vibrations are found at 1666(vs), 1608(vs) cm^{-1} in FT-IR and 1688(s), 1663(vs), 1624(vw), 1236(vs) cm^{-1} in FT-Raman respectively. The theoretical wavenumbers at 1666, 1661, 1615 and 1231 cm-1 are assigned as C-C stretching vibrations with PED contribution of 46, 46, 46 and 44% respectively.**Table -1:** Sample Table format

3.3 Hyperpolarizability calculation

NLO is at the future of current research because it provides the key functions of frequency shifting, optical modulation, optical switching, optical logic, and optical memory for the emerging technologies in areas such as telecommunications, signal processing, and optical interconnections [20, 21]. In discussing NLO properties, the polarization of the molecule by an external radiation field is often approximated as the creation of an induced dipole moment by an external electric field. The first hyperpolarizability (β_0) of this molecular system is calculated using B3LYP/6-311++G (d,p) method, based on the finite field approach.

The non-linear optical response of an isolated molecule in an electric field E_i (ω) can be represented as a Taylor series enlargement of the total dipole moment, μ_{tot}, induced by the field:

$$\mu_{tot} = \mu_0 + \alpha_{ij}E_j + \beta_{ijk}E_jE_k + \ldots,$$

Where α is the linear polarizability, μ_0 is the permanent dipole moment and β_{ijk} are the first hyperpolarizability tensor components. The isotropic (or average) linear polarizability is defined as:

$$\alpha = \frac{\alpha_{xx} + \alpha_{yy} + \alpha_{zz}}{3}$$

The first order hyperpolarizability is a third rank tensor that can be described by 3×3×3 matrix. The 27 components of 3D matrix can be abridged to 10 components owing to the Kleinman symmetry [20]
.Components of the first hyperpolarizability can be reckoned using the following equation:

$$\beta_i = \beta_{iii} + \sum_{i \neq j} (\beta_{ijj} + \beta_{jij} + \beta_{jji})$$

[d]Relative Raman intensities normalized to 100.

Using the x, y and z components of β, the magnitude of the first hyperpolarizability tensor can be calculated by:

$$\beta_{tot} = \sqrt{(\beta_x^2 + \beta_y^2 + \beta_z^2)}$$

The entire equation for reckoning the magnitude of β from Gaussian 09W program output is given a follows:

$$\beta_{tot} = \sqrt{(\beta_{xxx} + \beta_{xyy} + \beta_{xzz})^2 + (\beta_{yyy} + \beta_{yzz} + \beta_{xxy})^2 + (\beta_{zzz} + \beta_{xxz} + \beta_{yyz})^2}$$

The calculations of the total molecular dipole moment (μ), linear polarizability (α) and first-order hyperpolarizability (β) from the Gaussian output have been explained in detail previously[22], and DFT has been widely used as an efficient method to investigate the organic NLO materials [23, 24]. In addition, the polar properties of the P3P2E were computed at the DFT (B3LYP)/6-311++G(d,p) level using Gaussian 09W program package.

Urea is the prototypical molecule utilized in investigating of the NLO properties of the compound. For this reason, urea was used often as a threshold value for comparative purpose. The calculated dipole moment and hyperpolarizability values obtained from B3LYP/6-311++G(d,p) methods are collected in Table 3. The first order hyperpolarizability of P3P2E with B3LYP/6-311++G(d,p) basis set is 10.2210 x 10^{-30} sixteen times greater than the value of urea (βo = 0.6230 x 10^{-30} esu). From the computation, the high values of the hyperpolarizabilities of P3P2E are probably attributed to the charge transfer existing amid the benzene rings within the molecular skeleton. This is evidence for the nonlinear optical (NLO) property of the molecule.

Table -3: The values of calculated dipole moment, polarizability, first order hyperpolarizability (βtot) components of P3P2E

Parameters	B3LYP/6-311++G(d,p)	Parameters	B3LYP/6-311++G(d,p)
μ_x	-1.5752	β_{xxx}	-40.1292
μ_y	-0.0990	β_{xxy}	-12.4301
μ_z	-0.4749	β_{xyy}	-60.9058
μ(D)	1.6482	β_{yyy}	-2.1817
α_{xx}	225.0081	β_{zxx}	-181.5296
α_{xy}	7.8521	β_{xyz}	21.4969
α_{yy}	115.9279	β_{zyy}	46.8172
α_{xz}	-48.5794	β_{xzz}	432.6679
α_{yz}	3.4722	β_{yzz}	-57.4707
α_{zz}	201.9315	β_{zzz}	-998.6759
α(e.s.u)	2.6818x10^{-23}	βtot (e.s.u)	10.2210X10^{-30}
Δα(e.s.u)	201.9315 x10^{-23}		

3.4 Frontier molecular orbitals (FMOs)

The highest occupied molecular orbitals (HOMOs) and the lowest-lying unoccupied molecular orbitals (LUMOs) are named as frontier molecular orbitals (FMOs). The FMOs play an important role in the optical and electric properties, as well as in quantum chemistry and UV–vis. spectra [25]. HOMO-LUMO orbitals are also called frontier orbitals as they lie at the outermost boundaries of the electrons of the molecules. The frontier orbital gap helps characterize the chemical reactivity and the kinetic stability of the molecule. A molecule with a small frontier orbital gap is generally associated with a high chemical reactivity, low kinetic stability and is also termed as soft molecule [25]. The 3D plots of the frontier orbitals HOMO and LUMO figures for the P3P2E are shown in Fig. 5. The lowest unoccupied molecular orbital (LUMO) energy is -1.8389 eV and the highest occupied molecular orbital (HOMO) energy is -6.2790 eV. Lower value in the HOMO and LUMO energy gap explains the eventual charge transfer interactions taking place within the molecule, which influences the biological activity of the molecule. The narrow energy gap between HOMO and LUMO facilitates intra molecular charge transfer which makes the material to be NLO active [50]. Analysis of the wavefunction indicates that the electron absorption corresponds to the transition from the ground to the first excited state and is mainly described by one-electron excitation from the HOMO to the LUMO. All the HOMO and LUMO have nodes. The positive phase is red and the negative one is green. By using HOMO and LUMO energy values for a molecule, the chemical hardness, electronegativity, chemical potential and electrophilicity index of the molecule were calculated. The calculated results are presented in Table 4. Considering the chemical hardness, if a molecule has large HOMO–LUMO gap, it is a hard molecule or small HOMO–LUMO gap it is a soft molecule. One can also relate the stability of molecule to hardness, which means that the molecule with least HOMO–LUMO gap means it is more reactive.

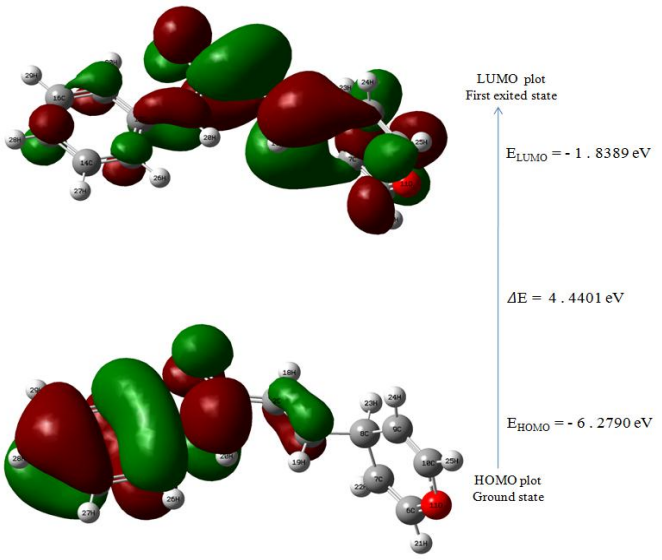

Fig -5: Highest occupied and lowest unoccupied molecular orbital of P3P2E obtain with B3LYP/6-311++G(d,p) method

3.5 Molecular electrostatic potential (MEP)

MEP and electrostatic potential are useful quantities to illustrate the charge distributions of molecules and used to visualize variably charged regions of a molecule. Therefore, the charge distributions can give information about how the molecules interact with another molecule. MEP is widely used as a reactivity map displaying most probable regions for the electrophilic attack of charged point-like reagents on organic molecules [26]. The molecular electrostatic potential V(r) that is created in the space around a molecule by its nuclei and electrons is well established as a guide to molecular reactive behavior. It is defined by:

$$V(r) = \sum Z_A \ / (R_A - r) \ - \int \rho(r')/(r'-r)dr'$$

Where the summation runs over all the nuclei A in the molecule and polarization and reorganization effects are neglected. ZA is the charge of the nucleus A, located at RA and ρ(r') is the electron density function of the molecule.

At any given point r(x, y, z) in the vicinity of a molecule, the MEP, V(r) is defined in terms of the interaction energy between the electrical charge generated from the molecule electrons and nuclei and a positive test charge (a proton) located at r [27]. The MEP is related to electron density and a very useful descriptor for determining sites for electrophilic attack and nucleophilic reactions as well as hydrogen-bonding interactions [28, 29]. To predict reactive sites for electrophilic and nucleophilic attack for the investigated molecule, the 3D Molecular electrostatic potential surface (MEPs) for the title molecule are shown in Figs. 6. The different values of the electrostatic potential at the surface are represented by different colors. Potential increases in the order red < orange < yellow < green < blue. The negative (red, orange and yellow) regions of the MEP are related to electrophilic reactivity. The MEP map shows that the negative potential sites are on electronegative oxygen atoms (O4 and O11) and the positive potential sites are around the hydrogen atoms. These sites give information about the region from where the compound can have intermolecular interactions. This predicted the most reactive site for both electrophilic and nucleophilic attack.

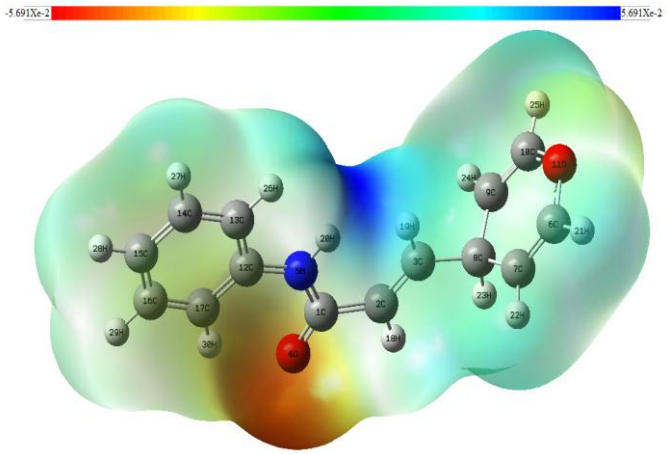

Fig -6: Molecular electrostatic potential of P3P2E calculated at B3LYP/6-311++G(d,p) basis set

3.6 Thermodynamic properties

On the basis of vibrational analysis at B3LYP/6-311++G(d,p) level, the standard statistical thermodynamic functions: heat capacity (C), entropy (S) and enthalpy (H) for the title compound were obtained from the theoretical harmonic frequencies and listed in Table 5. From Table 5, it can be observed that these thermodynamic functions are increasing with temperature ranging from 100 K to 700 K due to the fact that the molecular vibrational intensities increase with temperature [30]. The correlation equations between heat capacity, entropy, enthalpy and temperatures were fitted by quadratic formulas, and the corresponding fitting factors (R2) for these thermodynamic properties are 0.9997, 0.9999 and 0.9997, respectively. The corresponding fitting equations are as follows and the correlation graphics of those are shown in Fig. 7.

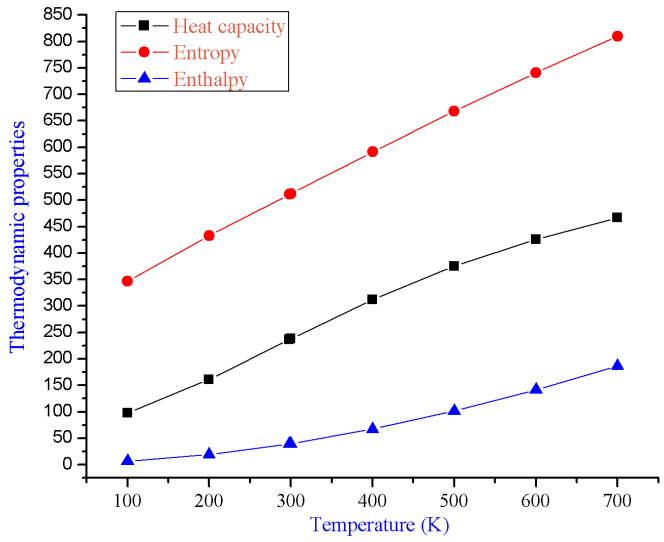

Fig -7: Correlation graphic of heat capacity, entropy, enthalpy and temperature for P3P2E

Table -4: Calculated energy values of title compound by B3LYP/6-311++G(d,p) method.

Basis set	B3LYP/6-311++G(d,p)
E_{Homo}(eV)	-6.279
E_{Lumo}(eV)	-1.8389
Ionization potential	6.279
Electron affinity	1.8389
Energy gap(eV)	4.4401
Electronegativity	4.05895
Chemical potential	-4.05895
Chemical hardness	2.22005
Chemical softness	0.22522
Electrophilicity index	3.710519

$(C^{0}_{p,m})$ = 6.1678 + 0.8755T – 3.0162 x $10^{-4}T^2$ (R^2 = 0.9997)

(S^{0}_{m}) = 259.6499 + 0.8890T –1.4608 x $10^{-4}T^2$(R^2 = 0.9999)

(H^{0}_{m}) = - 0.9842 + 0.0387T – 3.2910 x $10^{-4}T^2$ (R^2 = 0.9997)

All the thermodynamic data supply helpful information for the further study on the P3P2E. They can be used to compute the other thermodynamic energies according to relationships of thermodynamic functions and estimate directions of chemical reactions according to the second law of thermodynamics in thermo chemical field [30]. It must be noticed that all thermodynamic calculations were done in gas phase and they could not be used in solution.

Table -5: Temperature dependence of thermodynamic properties of P3P2E at B3LYP /6-311++G(d,P)

T(K)	$C^{0}_{p,m}$ (J/ mol K)	S^{0}_{m} (J/ mol K)	H^{0}_{m} (kJ/ mol)
100	98.04	346.73	6.86
200	161.09	432.97	19.66
298.15	236.39	511.13	39.12
300	237.83	512.59	39.56
400	312.25	591.42	67.14
500	375.11	668.09	101.61
600	425.75	741.13	141.75
700	466.47	809.92	186.43

4. CONCLUSIONS

FT-IR, FT-Raman and DFT quantum chemical calculations studies were performed on P3P2E, in order to identify its structural and spectroscopic features. Several properties were carried out using experimental techniques and tools derived from DFT. On the basis of experimental results and PED calculations, assignments of all the fundamental vibrational frequencies were done. A good correlation between the observed and scaled wavenumbers was obtained for the title compound. Scaled results seemed to be in good agreement with experimental ones. HUMO and LUMO orbitals have been visualize. It has been conclude that the lowest singlet excited state of the title molecule is mainly derived from the HOMO-LUMO electron transition. The electric dipole moment, polarizability, mean polarizability and the first order hyperpolarizability of the title compound were calculated. The correlations of the statistical thermodynamics according to temperature were also presented. We hope our results will be of assistance in the quest of the experimental and theoretical evidence for the title molecule in reaction intermediates, nonlinear optical and photoelectric materials and will also be helpful for the design and synthesis of new materials.

REFERENCES

[1] R. Matsubara, S. Kobayashi, “Enamides and Enecarbamates as Nucleophiles in Stereoselective C–C and C–N Bond-Forming Reactions”, Acc. Chem. Res, 41 (2008) 292-301.

[2] D.R. Carbery, "Enamides: valuable organic substrates", Org. Biomol. Chem. 6 (2008) 3455-3460.

[3] H. Mayr, "Structure–Nucleophilicity Relationships for Enamines", Chem. Eur. J. 2003, 9, 2003, 2209-2218.

[4] O. Èervinka, In The Chemistry of Enamines, Part 1; Rappoport, Z., Ed.; John Wiley & Sons: New York, 1994, Chap. 9, 467.

[5] G. Bélanger, M. Doré, F. Ménard, V.J. Darsigny, "Reactions of Aldehydes and Ketones and their Derivatives", Org. Chem, 71, 2006, 7481.

[6] S. Mukherjee, J.W. Yang, S. Hoffmann, "Asymmetric enamine catalysis", B List. Chem. Rev. 2007, 107, 5471-5569.

[7] T. Kuranaga, Y. Sesoko, M. Inoue, "Cu-mediated enamide formation in the total synthesis of complex peptide natural products", Nat. Prod. Rep, 31, 2014, 514-532.

[8] K. Okamoto, M. Sakagami, F. Feng, H. Togame, H. Takemoto, S. Ichikawa, A. Matsuda, "Total synthesis of pacidamycin D by Cu (I)-catalyzed oxy enamide formation", A. Org. Lett, 13, 2011, 5240-5243.

[9] K. Golcuk, A. Altun, M. Kumru, "Thermal studies and vibrational analyses of m-methylaniline complexes of Zn (II), Cd (II) and Hg (II) bromides", Spectrochim. Acta 59A (2003) 1841–1847.

[10] M. J. Frisch, G. W. Trucks, H. B. Schlegel, Gaussian 09, Revision **E.01,** Gaussian, Inc., Wallingford CT, 2009.

[11] N. Sundaraganesan, S. Illakiamani, H. Saleem, P.M. Wojciechowski, D. Michaliska, "FT-Raman and FT-IR spectra, vibrational assignments and density functional studies of 5-bromo-2-nitropyridine", Spectrochim. Acta A 61 (2005) 2995-3001.

[12] M.H. Jamroz, "Vibrational energy distribution analysis (VEDA): scopes and limitations", Spectrochim. Acta A 114 (2004) 220-230.

[13] A.M. Asiri, M. Akkurt, S. A. Khan, I. Ullah Khan and M.N. Arshad, "(E)-2-Cyano-3-[4-(dimethylamino)phenyl]- N -phenylprop-2-enamide", Acta Cryst. (2009). E65, o1303.

[14] N. Swarnalatha, S.Gunasekaran, S. Muthu, M. Nagarajan, "Molecular structure analysis and spectroscopic characterization of 9-methoxy-2H-furo[3,2-g]chromen-2-one with experimental (FT-IR and FT-Raman) techniques and quantum chemical calculations", spectrochim. Acta part A 137 (2015) 721-729.

[15] L.G. Wade (Ed), Advanced Organic Chemistry, 4th ed., Wiley, New York,1992. p.723.

[16] N. Sundaraganesan, S.Illakiamani, C. Meganathan, B.D. Joshua, "Vibrational spectroscopy investigation using ab initio and density functional theory analysis on the structure of 3-aminobenzotrifluoride", Spectrochim. Acta A 67 (2007) 214-224.

[17] Silverstein, G.C. Basseler, C. Morill, Spectrometric Identification of Organic Compounds, Wiley, New York, 1981.

[18] T. Gnanasambandan, S. Gunasekaran, and S. Seshadri, "Vibrational spectroscopic investigation on propylthiouracil, International Journal of Recent Scientific Research", 3 (2012) 590 – 597

[19] G. Varsanyi, Vibrational Spectra of Benzene Derivatives, Academic Press, NewYork, 1969.

[20] M. Raja, R. Raj Muhamed, S. Muthu, M. Suresh, "Synthesis, spectroscopic (FT-IR, FT-Raman, NMR, UV-Visible), NLO, NBO, HOMO-LUMO, Fukui function and molecular docking study of (E)-1-(5-bromo-2-hydroxybenzylidene)semicarbazide", Journal of Molecular Structure, 1141 (2017) 284–298.

[21] M. Szafran, A. komasa, E.B. Adamska, "Crystal and molecular structure of 4-carboxypiperidinium chloride (4-piperidinecarboxylic acid hydrochloride)", J Mol. Struct. THEOCHEM 827 (2007) 101-107.

[22] K.S. Thanthiri Watte, K. M. Nalin de silva, "Non-linear optical properties of novel fluorenyl derivatives-ab initio quantum chemical calculations", J. Mol. Struct. Theochem. 617 (2002) 169-175.

[23] S.G. Sagdinc, A. Esme, Spectrochim. "Theoretical and vibrational studies of 4, 5-diphenyl-2-2 oxazole propionic acid (oxaprozin)", Acta Part A 75 (2010) 1370-1380.

[24] S. Muthu, G. Ramachandran, "Spectroscopic studies (FTIR, FT-Raman and UV–Visible), normal coordinate analysis, NBO analysis", first order hyper polarizability, HOMO and LUMO analysis of (1R)-N-(Prop-2-yn-1-yl)-2,3-dihydro-1H-inden-1-amine molecule by ab initio HF and density functional methods Spectrochim. Acta part A 121, 2014, 394-403.

[25] I. Fleming, Frontier Orbitals and Organic Chemical Reactions, John Wiley & Sons, New York, 1976.

[26] P. Politzer, D.G. Truhlar (Eds.), Chemical Application of Atomic and Molecular Electrostatic Potentials, Plenum, New York, 1981.

[27] P. Politzer, J.S. Murray, "The fundamental nature and role of the electrostatic potential in atoms and molecules", Theor. Chem. Acc. 108, 2002, 134–142.

[28] F.J. Luque, J.M. Lopez, M. Orozco, "Perspective on Electrostatic interactions of a solute with a continuum. A direct utilization of ab initio molecular potentials for the prevision of solvent effects" Theor. Chem. Acc. 103, 2000, 343–345.

[29] N. Okulik, A.H. Jubert, "Theoretical analysis of the reactive sites of non-steroidal anti-inflammatory drugs", Internet Electron. J. Mol. Des. 4, 2005, 17–30.

[30] B. Otto, J. Boerio-Goates, Chemical Thermodynamics: Advanced Applications, Calculations from Statistical Thermodynamics, Academic Press, 2000.